Contrastive Multiview Coding

Yonglong Tian
MIT CSAIL
yonglong@mit.edu

Dilip Krishnan
Google Research
dilipkay@google.com

Phillip Isola
MIT CSAIL
phillipi@mit.edu

Abstract

Humans view the world through many sensory channels, e.g., the long-wavelength light channel, viewed by the left eye, or the high-frequency vibrations channel, heard by the right ear. Each view is noisy and incomplete, but important factors, such as physics, geometry, and semantics, tend to be shared between all views (e.g., a "dog" can be seen, heard, and felt). We investigate the classic hypothesis that a powerful representation is one that models view-invariant factors. We study this hypothesis under the framework of multiview contrastive learning, where we learn a representation that aims to maximize mutual information between different views of the same scene but is otherwise compact. Our approach scales to any number of views, and is view-agnostic. We analyze key properties of the approach that make it work, finding that the contrastive loss outperforms a popular alternative based on cross-view prediction, and that the more views we learn from, the better the resulting representation captures underlying scene semantics. Our approach achieves state-of-the-art results on image and video unsupervised learning benchmarks. Code is released at: http://github.com/HobbitLong/CMC/.

1. Introduction

A foundational idea in coding theory is to learn compressed representations that nonetheless can be used to reconstruct the raw data. This idea shows up in contemporary representation learning in the form of autoencoders [65] and generative models [40, 24], which try to represent a data point or distribution as losslessly as possible. Yet lossless representation might not be what we really want, and indeed it is trivial to achieve – the raw data itself is a lossless representation. What we might instead prefer is to keep the "good" information (signal) and throw away the rest (noise). How can we identify what information is signal and what is noise?

To an autoencoder, or a max likelihood generative model, a bit is a bit. No one bit is better than any other. Our conjecture in this paper is that some bits *are* in fact better than others. Some bits code important properties like semantics, physics, and geometry, while others code attributes that we might consider less important, like incidental lighting conditions or thermal noise in a camera's sensor.

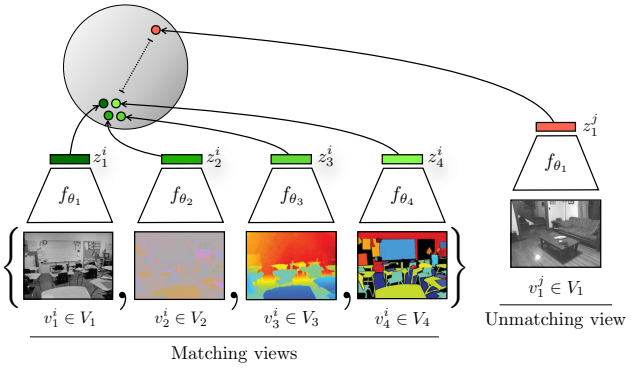

Figure 1: Given a set of sensory views, a deep representation is learnt by bringing views of the *same* scene together in embedding space, while pushing views of *different* scenes apart. Here we show and example of a 4-view dataset (NYU RGBD [53]) and its learned representation. The encodings for each view may be concatenated to form the full representation of a scene.

We revisit the classic hypothesis that the good bits are the ones that are shared between multiple *views* of the world, for example between multiple sensory modalities like vision, sound, and touch [70]. Under this perspective "presence of dog" is good information, since dogs can be seen, heard, and felt, but "camera pose" is bad information, since a camera's pose has little or no effect on the acoustic and tactile properties of the imaged scene. This hypothesis corresponds to the inductive bias that the way you view a scene should not affect its semantics. There is significant evidence in the cognitive science and neuroscience literature that such view-invariant representations are encoded by the brain (e.g., [70, 15, 32]). In this paper, we specifically study the setting where the different views are different image channels, such as luminance, chrominance, depth, and optical flow. The fundamental supervisory signal we exploit is the *co-occurrence*, in natural data, of multiple views of the same scene. For example, we consider an image in Lab color space to be a paired example of the co-occurrence of two views of the scene, the L view and the ab view: $\{L, ab\}$.

Our goal is therefore to learn representations that capture

information shared between multiple sensory channels but that are otherwise compact (i.e. discard channel-specific nuisance factors). To do so, we employ contrastive learning, where we learn a feature embedding such that views of the same scene map to nearby points (measured with Euclidean distance in representation space) while views of different scenes map to far apart points. In particular, we adapt the recently proposed method of Contrastive Predictive Coding (CPC) [57], except we simplify it – removing the recurrent network – and generalize it – showing how to apply it to arbitrary collections of image channels, rather than just to temporal or spatial predictions. In reference to CPC, we term our method *Contrastive Multiview Coding* (CMC), although we note that our formulation is arguably equally related to Instance Discrimination [79]. The contrastive objective in our formulation, as in CPC and Instance Discrimination, can be understood as attempting to maximize the mutual information between the representations of multiple views of the data.

We intentionally leave "good bits" only loosely defined and treat its definition as an empirical question. Ultimately, the proof is in the pudding: we consider a representation to be good if it makes subsequent problem solving easy, on tasks of human interest. For example, a useful representation of images might be a feature space in which it is easy to learn to recognize objects. We therefore evaluate our method by testing if the learned representations transfer well to standard semantic recognition tasks. On several benchmark tasks, our method achieves results competitive with the state of the art, compared to other methods for self-supervised representation learning. We additionally find that the quality of the representation improves as a function of the number of views used for training. Finally, we compare the contrastive formulation of multiview learning to the recently popular approach of cross-view prediction, and find that in head-to-head comparisons, the contrastive approach learns stronger representations.

The core ideas that we build on: contrastive learning, mutual information maximization, and deep representation learning, are not new and have been explored in the literature on representation and multiview learning for decades [64, 45, 80, 3]. Our main contribution is to set up a framework to extend these ideas to *any number of views*, and to empirically study the factors that lead to success in this framework. A review of the related literature is given in Section 2; and Fig. 1 gives a pictorial overview of our framework. Our main contributions are:

- We apply contrastive learning to the multiview setting, attempting to maximize mutual information between representations of different views of the same scene (in particular, between different image channels).
- We extend the framework to learn from *more than two* views, and show that the quality of the learned representation improves as number of views increase. Ours is the first work to explicitly show the benefits of multiple views on representation quality.
- We conduct controlled experiments to measure the effect of mutual information estimates on representation quality. Our experiments show that the relationship between mutual information and views is a subtle one.
- Our representations rival state of the art on popular benchmarks.
- We demonstrate that the contrastive objective is superior to cross-view prediction.

2. Related work

Unsupervised representation learning is about learning transformations of the data that make subsequent problem solving easier [7]. This field has a long history, starting with classical methods with well established algorithms, such as principal components analysis (PCA [37]) and independent components analysis (ICA [33]). These methods tend to learn representations that focus on low-level variations in the data, which are not very useful from the perspective of downstream tasks such as object recognition.

Representations better suited to such tasks have been learnt using deep neural networks, starting with seminal techniques such as Boltzmann machines [71, 65], autoencoders [30], variational autoencoders [40], generative adversarial networks [24] and autoregressive models [56]. Numerous other works exist, for a review see [7]. A powerful family of models for unsupervised representations are collected under the umbrella of "self-supervised" learning [64, 35, 85, 84, 78, 60, 83]. In these models, an input X to the model is transformed into an output $\hat{X}$, which is supposed to be close to another signal Y (usually in Euclidean space), which itself is related to X in some meaningful way. Examples of such X/Y pairs are: luminance and chrominance color channels of an image [85], patches from a single image [57], modalities such as vision and sound [58] or the frames of a video [78]. Clearly, such examples are numerous in the world, and provides us with nearly infinite amounts of training data: this is one of the appeals of this paradigm. Time contrastive networks [68] use a triplet loss framework to learn representations from aligned video sequences of the same scene, taken by different video cameras. Closely related to self-supervised learning is the idea of multi-view learning, which is a general term involving many different approaches such as co-training [8], multi-kernel learning [13] and metric learning [6, 87]; for comprehensive surveys please see [80, 45]. Nearly all existing works have dealt with one or two views such as video or image/sound. However, in many situations, many more views are available to provide training signals for any representation.

The objective functions used to train deep learning based representations in many of the above methods are either

reconstruction-based loss functions such as Euclidean losses in different norms e.g. [34], adversarial loss functions [24] that learn the loss in addition to the representation, or contrastive losses e.g. [26, 81, 72, 25, 31, 57, 3, 29, 36] that take advantage of the co-occurence of multiple views.

Some of the prior works most similar to our own (and inspirational to us) are Contrastive Predictive Coding (CPC) [57], Deep InfoMax [31], and Instance Discrimination [79]. These methods, like ours, learn representations by contrasting between congruent and incongruent representations of a scene. CPC learns from two views – the past and future – and is applicable to sequential data, either in space or in time. Deep Infomax [31] considers the two views to be the input to a neural network and its output. Instance Discrimination learns to match two sub-crops of the same image. CPC and Deep InfoMax have recently been extended in [29] and [4] respectively. These methods all share similar mathematical objectives, but differ in the definition of the views. Our method differs from these works in the following ways: we extend the objective to the case of *more than two* views, and we explore a different set of view definitions, architectures, and application settings. In addition, we contribute a unique empirical investigation of this paradigm of representation learning.

The idea of contrastive learning has also started to spread over many other tasks in various other domains [74, 86, 61, 76, 48, 38, 75].

3. Method

Our goal is to learn representations that capture information shared between multiple sensory views without human supervision. We start by reviewing previous predictive learning (or reconstruction-based learning) methods, and then elaborate on contrastive learning within two views. We show connections to mutual information maximization and extend it to scenarios including more than two views. We consider a collection of M views of the data, denoted as $V_1, \ldots, V_M$. For each view V_i, we denote v_i as a random variable representing samples following $v_i \sim \mathcal{P}(V_i)$.

3.1. Predictive Learning

Let V_1 and V_2 represent two views of a dataset. For instance, V_1 might be the luminance of a particular image and V_2 the chrominance. We define the *predictive learning* setup as a deep nonlinear transformation from v_1 to v_2 through latent variables z, as shown in Fig. 2. Formally, $z = f(v_1)$ and $\hat{v_2} = g(z)$, where f and g represent the encoder and decoder respectively and $\hat{v_2}$ is the prediction of v_2 given v_1. The parameters of the encoder and decoder models are then trained using an objective function that tries to bring $\hat{v_2}$ "close to" v_2. Simple examples of such an objective include the $\mathcal{L}_1$ or $\mathcal{L}_2$ loss functions. Note that these objectives assume independence between each pixel or element of v_2 given v_1,

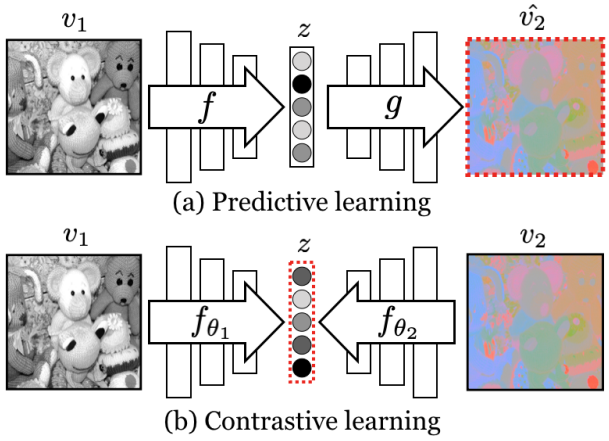

Figure 2: Predictive Learning vs Contrastive Learning. Cross-view prediction (**Top**) learns latent representations that predict one view from another, with loss measured in the *output* space. Common prediction losses, such as the $\mathcal{L}_1$ and $\mathcal{L}_2$ norms, are *unstructured*, in the sense that they penalize each output dimension independently, perhaps leading to representations that do not capture all the shared information between the views. In contrastive learning (**Bottom**), representations are learnt by contrasting congruent and incongruent views, with loss measured in *representation* space. The red dotted outlines show where the loss function is applied.

i.e., $p(v_2|v_1) = \Pi_i p(v_{2i}|v_1)$, thereby reducing their ability to model correlations or complex structure. The predictive approach has been extensively used in representation learning, for example, colorization [84, 85] and predicting sound from vision [58].

3.2. Contrastive Learning with Two Views

The idea behind contrastive learning is to learn an embedding that separates (contrasts) samples from two different distributions. Given a dataset of V_1 and V_2 that consists of a collection of samples $\{v_1^i, v_2^i\}_{i=1}^N$, we consider contrasting congruent and incongruent pairs, i.e. samples from the joint distribution $x \sim p(v_1, v_2)$ or $x = \{v_1^i, v_2^i\}$, which we call *positives*, versus samples from the product of marginals, $y \sim p(v_1)p(v_2)$ or $y = \{v_1^i, v_2^j\}$, which we call *negatives*.

We learn a "critic" (a discriminating function) $h_\theta(\cdot)$ which is trained to achieve a high value for positive pairs and low for negative pairs. Similar to recent setups for contrastive learning [57, 25, 51], we train this function to correctly select a single positive sample x out of a set $S = \{x, y_1, y_2, ..., y_k\}$ that contains k negative samples:

$$\mathcal{L}_{contrast} = -\mathop{\mathbb{E}}_{S}\left[\log \frac{h_\theta(x)}{h_\theta(x) + \sum_{i=1}^{k} h_\theta(y_i)}\right] \quad (1)$$

To construct S, we simply fix one view and enumerate positives and negatives from the other view, allowing us to

rewrite the objective as:

$$\mathcal{L}_{contrast}^{V_1,V_2} = - \mathop{\mathbb{E}}_{\{v_1^1, v_2^1, \ldots, v_2^{k+1}\}} \left[\log \frac{h_\theta(\{v_1^1, v_2^1\})}{\sum_{j=1}^{k+1} h_\theta(\{v_1^1, v_2^j\})} \right] \quad (2)$$

where k is the number of negative samples v_2^j for a given sample v_1^1. In practice, k can be extremely large (e.g., 1.2 million in ImageNet), and so directly minimizing Eq. 2 is infeasible. In Section 3.4, we show two approximations that allow for tractable computation.

Implementing the critic We implement the critic $h_\theta(\cdot)$ as a neural network. To extract compact latent representations of v_1 and v_2, we employ two encoders $f_{\theta_1}(\cdot)$ and $f_{\theta_2}(\cdot)$ with parameters θ_1 and θ_2 respectively. The latent representions are extracted as $z_1 = f_{\theta_1}(v_1)$, $z_2 = f_{\theta_2}(v_2)$. We compute their cosine similarity as score and adjust its dynamic range by a hyper-parameter τ:

$$h_\theta(\{v_1, v_2\}) = \exp\left(\frac{f_{\theta_1}(v_1) \cdot f_{\theta_2}(v_2)}{\|f_{\theta_1}(v_1)\| \cdot \|f_{\theta_2}(v_2)\|} \cdot \frac{1}{\tau}\right) \quad (3)$$

Loss $\mathcal{L}_{contrast}^{V_1,V_2}$ in Eq. 2 treats view V_1 as anchor and enumerates over V_2. Symmetrically, we can get $\mathcal{L}_{contrast}^{V_2,V_1}$ by anchoring at V_2. We add them up as our two-view loss:

$$\mathcal{L}(V_1, V_2) = \mathcal{L}_{contrast}^{V_1,V_2} + \mathcal{L}_{contrast}^{V_2,V_1} \quad (4)$$

After the contrastive learning phase, we use the representation z_1, z_2, or the concatenation of both, $[z_1, z_2]$, depending on our paradigm. This process is visualized in Fig. 1.

Connecting to mutual information The optimal critic h_θ^* is proportional to the density ratio between the joint distribution $p(z_1, z_2)$ and the product of marginals $p(z_1)p(z_2)$ (proof provided in supplementary material):

$$h_\theta^*(\{v_1, v_2\}) \quad \propto \quad \frac{p(z_1, z_2)}{p(z_1)p(z_2)} \propto \frac{p(z_1|z_2)}{p(z_1)} \quad (5)$$

This quantity is the pointwise mutual information, and its expectation, in Eq. 2, yields an estimator related to mutual information. A formal proof is given by [57, 62], which we recapitulate in supplement, showing that:

$$I(z_i; z_j) \geq \log(k) - \mathcal{L}_{contrast} \quad (6)$$

where, as above, k is the number of negative pairs in sample set S. Hence minimizing the objective $\mathcal{L}$ maximizes the lower bound on the mutual information $I(z_i; z_j)$, which is bounded above by $I(v_i; v_j)$ by the data processing inequality. The dependency on k also suggests that using more negative samples can lead to an improved representation; we show that this is indeed the case (see supplement). We note that recent work [47] shows that the bound in Eq. 6 can be very weak; and finding better estimators of mutual information is an important open problem.

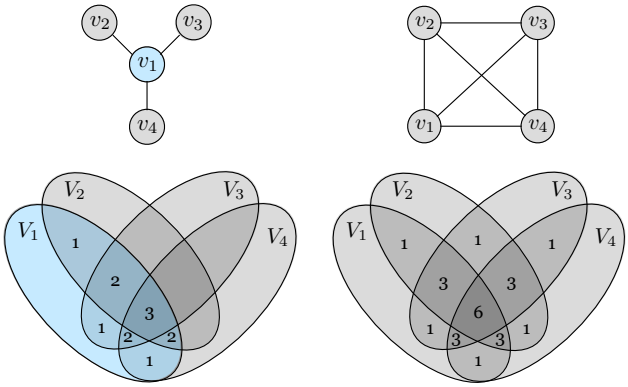

(a) Core View (b) Full Graph

Figure 3: Graphical models and information diagrams [1] associated with the core view and full graph paradigms, for the case of 4 views, which gives a total of 6 learning objectives. The numbers within the regions show how much "weight" the total loss places on each partition of information (i.e. how many of the 6 objectives that partition contributes to). A region with no number corresponds to 0 weight. For example, in the full graph case, the mutual information between all 4 views is considered in all 6 objectives, and hence is marked with the number 6.

3.3. Contrastive Learning with More than Two Views

We present more general formulations of Eq. 2 that can handle any number of views. We call them the "core view" and "full graph" paradigms, which offer different tradeoffs between efficiency and effectiveness. These formulations are visualized in Fig. 3.

Suppose we have a collection of M views $V_1, \ldots, V_M$. The "core view" formulation sets apart one view that we want to optimize over, say V_1, and builds pair-wise representations between V_1 and each other view $V_j, j > 1$, by optimizing the sum of a set of pair-wise objectives:

$$\mathcal{L}_C = \sum_{j=2}^{M} \mathcal{L}(V_1, V_j) \quad (7)$$

A second, more general formulation is the "full graph" where we consider all pairs $(i, j), i \neq j$, and build $\binom{n}{2}$ relationships in all. By involving all pairs, the objective function that we optimize is:

$$\mathcal{L}_F = \sum_{1 \leq i < j \leq M} \mathcal{L}(V_i, V_j) \quad (8)$$

Both these formulations have the effect that information is prioritized in proportion to the number of views that share that information. This can be seen in the information diagrams visualized in Fig. 3. The number in each partition of the diagram indicates how many of the pairwise objectives, $\mathcal{L}(V_i, V_j)$, that partition contributes to. Under both the core

view and full graph objectives, a factor, like "presence of dog", that is common to all views will be preferred over a factor that affects fewer views, such as "depth sensor noise".

The computational cost of the bivariate score function in the full graph formulation is combinatorial in the number of views. However, it is clear from Fig. 3 that this enables the full graph formulation to capture more information between different views, which may prove useful for downstream tasks. For example, the mutual information between V_2 and V_3 or V_2 and V_4 is completely ignored in the core view paradigm (as shown by a 0 count in the information diagram). Another benefit of the full graph formulation is that it can handle missing information (e.g. missing views) in a natural manner.

3.4. Implementing the Contrastive Loss

Better representations using $\mathcal{L}_{contrast}^{V_1,V_2}$ in Eqn. 2 are learnt by using many negative samples. In the extreme case, we include every data sample in the denominator for a given dataset. However, computing the full softmax loss is prohibitively expensive for large dataset such as ImageNet. One way to approximate this full softmax distribution, as well as alleviate the computational load, is to use Noise-Contrastive Estimation [25, 79] (see supplement). Another solution, which we also adopt here, is to randomly sample m negatives and do a simple (m+1)-way softmax classification. This strategy is also used in [4, 29, 27] and dates back to [72].

Memory bank. Following [79], we maintain a memory bank to store latent features for each training sample. Therefore, we can efficiently retrieve m negative samples from the memory buffer to pair with each positive sample without recomputing their features. The memory bank is dynamically updated with features computed on the fly. The benefit of a memory bank is to allow contrasting against more negative pairs, at the cost of slightly stale features.

4. Experiments

We extensively evaluate Contrastive Multiview Coding (CMC) on a number of datasets and tasks. We evaluate on two established image representation learning benchmarks: ImageNet [16] and STL-10 [12] (see supplement). We further validate our framework on video representation learning tasks, where we use image and optical flow modalities, as the two views that are jointly learned. The last set of experiments extends our CMC framework to more than two views and provides empirical evidence of its effectiveness.

4.1. Benchmarking CMC on ImageNet

Following [84], we evaluate task generalization of the learned representation by training 1000-way *linear* classifiers on top of different layers. This is a standard benchmark that has been adopted by many papers in the literature.

Setting	ResNet-50 x0.5	ResNet-50 x1	ResNet-50 x2
$\{L, ab\}$	57.5 / 80.3	64.0 / 85.5	68.3 / 88.2
$\{Y, DbDr\}$	58.4 / 81.2	64.8 / 86.1	69.0 / 88.9
$\{Y, DbDr\}$ + RA	**60.0 / 82.3**	**66.2 / 87.0**	**70.6 / 89.7**

Table 1: Top-1 / Top-5 *Single* crop classification accuracy (%) on ImageNet with a supervised logistic regression classifier. We evaluate CMC using ResNet50 with different width as encoder for *each* of the two views (e.g., *L* and *ab*). "RA" stands for RandAugment [14].

Setup. Given a dataset of RGB images, we convert them to the *Lab* image color space, and split each image into *L* and *ab* channels, as originally proposed in SplitBrain autoencoders [85]. During contrastive learning, L and ab from the same image are treated as the positive pair, and ab channels from other randomly selected images are treated as a negative pair (for a given L). Each split represents a view of the orginal image and is passed through a separate encoder. As in SplitBrain, we design these two encoders by evenly splitting a given deep network, such as AlexNet [43], into sub-networks across the channel dimension. By concatenating representations layer-wise from these two encoders, we achieve the final representation of an input image. As proposed by previous literature [57, 31, 3, 87, 79], the quality of such a representation is evaluated by freezing the weights of encoder and training linear classifier on top of each layer.

Implementation. Unless otherwise specified, we use PyTorch [59] default data augmentation. Following [79], we set the temperature τ as 0.07 and use a momentum 0.5 for memory update. We use 16384 negatives. The supplementary material provides more details on our hyperparameter settings.

CMC with AlexNet. As many previous unsupervised methods are evaluated with AlexNet [43] on ImageNet [16, 42, 17, 84, 54, 18, 85, 55, 22, 11, 83], we also include the the results of CMC using this network. Due to the space limit, we present this comparison in supplementary material.

CMC with ResNets. We verify the effectiveness of CMC with larger networks such as ResNets [28]. We experiment on learning from luminance and chrominance views in two colorspaces, $\{L, ab\}$ and $\{Y, DbDr\}$ (see sec. 4.4 for validation of this choice), and we vary the width of the ResNet encoder for each view. We use the feature after the global pooling layer to train the linear classifier, and the results are shown in Table 1. $\{L, ab\}$ achieves 68.3% top-1 single crop accuracy with ResNet50x2 for each view, and switching to $\{Y, DbDr\}$ further brings about 0.7% improvement. On top of it, strengthening data augmentation with RandAugment [14] yields better or comparable results to other state-of-the-art methods [41, 79, 87, 27, 49, 19, 29, 4].

Method	# of Views	UCF-101	HMDB-51
Random	-	48.2	19.5
ImageNet	-	67.7	28.0
VGAN* [77]	2	52.1	-
LT-Motion* [46]	2	53.0	-
TempCoh [52]	1	45.4	15.9
Shuffle and Learn [50]	1	50.2	18.1
Geometry [21]	2	55.1	23.3
OPN [44]	1	56.3	22.1
ST Order [10]	1	58.6	25.0
Cross and Learn [66]	2	58.7	**27.2**
CMC (V)	2	55.3	-
CMC (D)	2	57.1	-
CMC (V+D)	3	**59.1**	26.7

Table 2: Test accuracy (%) on UCF-101 which evaluates *task* transferability and on HMDB-51 which evaluates *task* and *dataset* transferability. Most methods either use single RGB view or additional optical flow view, while VGAN explores sound as the second view. * indicates different network architecture.

4.2. CMC on videos

We apply CMC on videos by drawing insight from the two-streams hypothesis [67, 23], which posits that human visual cortex consists of two distinct processing streams: the ventral stream, which performs object recognition, and the dorsal stream, which processes motion. In our formulation, given an image i_t that is a frame centered at time t, the ventral stream associates it with a neighbouring frame i_{t+k}, while the dorsal stream connects it to optical flow f_t centered at t. Therefore, we extract i_t, i_{t+k} and f_t from two modalities as three views of a video; for optical flow we use the TV-L1 algorithm [82]. Two separate contrastive learning objectives are built within the ventral stream (i_t, i_{t+k}) and within the dorsal stream (i_t, f_t). For the ventral stream, the negative sample for i_t is chosen as a random frame from another randomly chosen video; for the dorsal stream, the negative sample for i_t is chosen as the flow corresponding to a random frame in another randomly chosen video.

Pre-training. We train CMC on UCF101 [73] and use two CaffeNets [43] for extracting features from images and optical flows, respectively. In our implementation, f_t represents 10 continuous flow frames centered at t. We use batch size of 128 and contrast each positive pair with 127 negative pairs.

Action recognition. We apply the learnt representation to the task of action recognition. The spatial network from [69] is a well-established paradigm for evaluating pre-trained RGB network on action recognition task. We follow the same spirit and evaluate the transferability of our RGB CaffeNet on UCF101 and HMDB51 datasets. We initialize the action recognition CaffeNet up to conv5 using the weights from the pre-trained RGB CaffeNet. The averaged accuracy over three splits is present in Table 2. Unifying both ventral and dorsal streams during pre-training produces higher accuracy for downstream recognition than using only single stream. Increasing the number of views of the data from 2 to 3 (using both streams instead of one) provides a boost for UCF-101.

4.3. Extending CMC to More Views

We further extend our CMC learning framework to multi-view scenarios. We experiment on the NYU-Depth-V2 [53] dataset which consists of 1449 labeled images. We focus on a deeper understanding of the behavior and effectiveness of CMC. The views we consider are: luminance (L channel), chrominance (ab channel), depth, surface normal [20], and semantic labels.

Setup. To extract features from each view, we use a neural network with 5 convolutional layers, and 2 fully connected layers. As the size of the dataset is relatively small, we adopt the sub-patch based contrastive objective (see supplement) to increase the number of negative pairs. Patches with a size of 128×128 are randomly cropped from the original images for contrastive learning (from images of size 480×640). For downstream tasks, we discard the fully connected layers and evaluate using the convolutional layers as a representation.

4.3.1 Does representation quality improve as number of views increases?

To measure the quality of the learned representation, we consider the task of predicting semantic labels from the representation of L. We follow the *core view paradigm* and use L as the core view, thus learning a set of representations by contrasting different views with L. A UNet style architecture [63] is utilized to perform the segmentation task. Contrastive training is performed on the above architecture that is equivalent of the UNet's encoder. After contrastive training is completed, we initialize the encoder weights of the UNet from the L encoder (which are equivalent architectures) and keep them frozen. Only the decoder is trained during this finetuning stage.

Since we use the patch-based contrastive loss, in the 1 view setting case, CMC coincides with DIM [31]. The 2-4 view cases contrast L with ab, and then sequentially add depth and surface normals. The semantic labeling results are measured by mean IoU over all classes and pixel accuracy, shown in Fig. 4. We see that the performance steadily improves as new views are added. We have tested different orders of adding the views, and they all follow a similar pattern.

We also compare CMC with two baselines. First, we randomly initialize and freeze the encoder, and we call this the *Random* baseline; it serves as a lower bound on the quality since the representation is just a random projection. Rather than freezing the randomly initialized encoder, we could

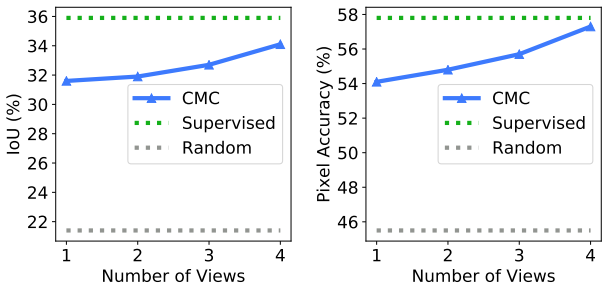

Figure 4: We show the Intersection over Union (IoU) (left) and Pixel Accuracy (right) for the NYU-Depth-V2 dataset, as CMC is trained with increasingly more views from 1 to 4. As more views are added, both these metrics steadily increase. The views are (in order of inclusion): L, ab, depth and surface normals.

	Pixel Accuracy (%)	mIoU (%)
Random	45.5	21.4
CMC (core-view)	57.1	34.1
CMC (full-graph)	57.0	34.4
Supervised	**57.8**	**35.9**

Table 3: Results on the task of predicting semantic labels from **L channel** representation which is learnt using the patch-based contrastive loss and all 4 views. We compare CMC with *Random* and *Supervised* baselines, which serve as lower and upper bounds respectively. Th core-view paradigm refers to Fig. 3(a), and full-view Fig. 3(b).

train it jointly with the decoder. This end-to-end *Supervised* baseline serves as an upper bound. The results are presented in Table 3, which shows our CMC produces high quality feature maps even though it's unaware of the downstream task.

4.3.2 Is CMC improving all views?

A desirable unsupervised representation learning algorithm operating on multiple views or modalities should improve the quality of representations for all views. We therefore investigate our CMC framwork beyond L channel. To treat all views fairly, we train these encoders following the *full graph paradigm*, where each view is contrasted with all other views.

We evaluate the representation of each view v by predicting the semantic labels from only the representation of v, where v is L, ab, depth or surface normals. This uses the full-graph paradigm. As in the previous section, we compare CMC with *Random* and *Supervised* baselines. As shown in Table 4, the performance of the representations learned by CMC using full-graph significantly outperforms that of randomly projected representations, and approaches the performance of the fully supervised representations. Furthermore, the full-graph representation provides a good representation

	Metric (%)	L	ab	Depth	Normal
Random	mIoU	21.4	15.6	30.1	29.5
	pix. acc.	45.5	37.7	51.1	50.5
CMC	mIoU	34.4	26.1	39.2	37.8
	pix. acc.	57.0	49.6	**59.4**	57.8
Supervised	mIoU	**35.9**	**29.6**	**41.0**	**41.5**
	pix. acc.	**57.8**	**52.6**	59.1	**59.6**

Table 4: Performance on the task of using single view v to predict the semantic labels, where v can be L, ab, depth or surface normal. Our CMC framework improves the quality of unsupervised representations towards that of supervised ones, for all of views investigated. This uses the full-graph paradigm Fig. 3(b).

	Accuracy on STL-10 (%)	
Views	Predictive	Contrastive
L, Depth	55.5	**58.3**
L, Normal	58.4	**60.1**
L, Seg. Map	57.7	**59.2**
Random	25.2	
Supervised	65.1	

Table 5: We compare predictive learning with contrastive learning by evaluating the learned encoder on unseen dataset and task. The contrastive learning framework consistently outperforms predictive learning.

learnt for all views, showing the importance of capturing different types of mutual information across views.

4.3.3 Predictive Learning vs. Contrastive Learning

While experiments in section 4.1 show that contrastive learning outperforms predictive learning [85] in the context of Lab color space, it's unclear whether such an advantage is due to the natural inductive bias of the task itself. To further understand this, we go beyond chrominance (ab), and try to answer this question when geometry or semantic labels are present.

We consider three view pairs on the NYU-Depth dataset: (1) L and depth, (2) L and surface normals, and (3) L and segmentation map. For each of them, we train two identical encoders for L, one using contrastive learning and the other with predictive learning. We then evaluate the representation quality by training a linear classifier on top of these encoders on the STL-10 dataset.

The comparison results are shown in Table 5, which shows that contrastive learning consistently outperforms predictive learning in this scenario where both the task and the dataset are unknown. We also include "random" and "supervised" baselines similar to that in previous sections. Though in the unsupervised stage we only use 1.3K images from a dataset much different from the target dataset STL-10,

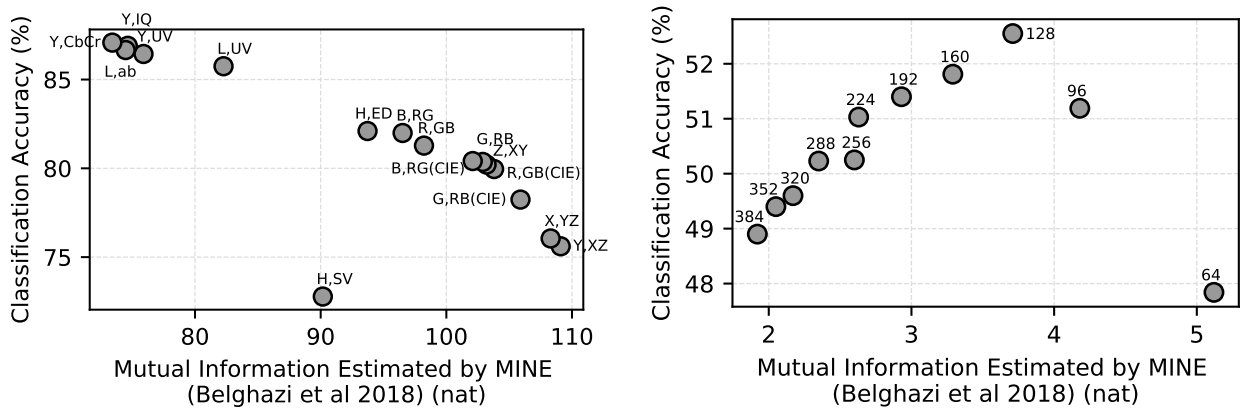

Figure 5: How does mutual information between views relate to representation quality? (Left) Classification accuracy against estimated MI between channels of different color spaces; (Right) Classification accuracy vs estimated MI between patches at different distances (distance in pixels is denoted next to each data point). MI estimated using MINE [5].

the object recognition accuracy is close to the supervised method, which uses an end-to-end deep network directly trained on STL-10.

Given two views V_1 and V_2 of the data, the predictive learning approach approximately models $p(v_2|v_1)$. Furthermore, losses used typically for predictive learning, such as pixel-wise reconstruction losses usually impose an independence assumption on the modeling: $p(v_2|v_1) \approx \Pi_i p(v_{2i}|v_1)$. On the other hand, the contrastive learning approach by construction does not assume conditional independence across dimensions of v_2. In addition, the use of random jittering and cropping between views allows the contrastive learning approach to benefit from spatial co-occurrence (contrasting in space) in addition to contrasting across views. We conjecture that these are two reasons for the superior performance of contrastive learning approaches over predictive learning.

4.4. How does mutual information affect representation quality?

Given a fixed set of views, CMC aims to maximize the mutual information between representations of these views. We have found that maximizing information in this way indeed results in strong representations, but it would be incorrect to infer that information maximization (infomax) is the key to good representation learning. In fact, this paper argues for precisely the opposite idea: that cross-view representation learning is effective because it results in a kind of information minimization, *discarding* nuisance factors that are not shared between the views.

The resolution to this apparent dilemma is that we want to maximize the "good" information – the *signal* – in our representations, while minimizing the "bad" information – the *noise*. The idea behind CMC is that this can be achieved by doing infomax learning on two views that share signal but have independent noise. This suggests a "Goldilocks principle" [39]: a good collection of views is one that shares some information but not too much. Here we test this hypothesis on two domains: learning representations on images with different colorspaces forming the two views; and learning representations on pairs of patches extracted from an image, separated by varying spatial distance.

In patch experiments we randomly crop two RGB patches of size 64x64 from the same image, and use these patches as the two views. Their relative position is fixed. Namely, the two patches always starts at position (x, y) and $(x+d, y+d)$ with (x, y) being randomly sampled. While varying the distance d, we start from 64 to avoid overlapping. There is a possible bias that with an image of relatively small size (e.g., 512x512), a large d (e.g., 384) will always push these two patches around boundary. To minimize this bias, we use high resolution images (e.g. $2k$) from DIV2K [2] dataset.

Fig. 5 shows the results of these experiments. The left plot shows the result of learning representations on different colorspaces (splitting each colorspace into two views, such as (L, ab), (R, GB) etc). We then use the MINE estimator [5] to estimate the mutual information between the views. We measure representation quality by training a linear classifier on the learned representations on the STL-10 dataset [12]. The plots clearly show that using colorspaces with minimal mutual information give the best downstream accuracy (For the outlier HSV in this plot, we conjecture the representation quality is harmed by the periodicity of H. Note that the H in HED is not periodic.). On the other hand, the story is more nuanced for representations learned between patches at different offsets from each other (Fig. 5, right). Here we see that views with too little or too much MI perform worse; a sweet spot in the middle exists which gives the best representation. That there exists such a sweet spot should be

expected. If two views share *no* information, then, in principle, there is no incentive for CMC to learn anything. If two views share all their information, no nuisances are discarded and we arrive back at something akin to an autoencoder or generative model, that simply tries to represent all the bits in the multiview data.

These experiments demonstrate that the relationship between mutual information and representation quality is meaningful but not direct. Selecting optimal views, which just share relevant signal, may be a fruitful direction for future research.

5. Conclusion

We have presented a contrastive learning framework which enables the learning of unsupervised representations from multiple views of a dataset. The principle of maximization of mutual information enables the learning of powerful representations. A number of empirical results show that our framework performs well compared to predictive learning and scales with the number of views.

Acknowledgements Thanks to Devon Hjelm for providing implementation details of Deep InfoMax, Zhirong Wu and Richard Zhang for helpful discussion and comments. This material is based on resources supported by Google Cloud.

References

[1] Information Diagram - Wikipedia. https://en.wikipedia.org/wiki/Information_diagram. 4

[2] Eirikur Agustsson and Radu Timofte. Ntire 2017 challenge on single image super-resolution: Dataset and study. In *CVPR*, 2017. 8

[3] Sanjeev Arora, Hrishikesh Khandeparkar, Mikhail Khodak, Orestis Plevrakis, and Nikunj Saunshi. A theoretical analysis of contrastive unsupervised representation learning. In *ICML*, 2019. 2, 3, 5

[4] Philip Bachman, R Devon Hjelm, and William Buchwalter. Learning representations by maximizing mutual information across views. *arXiv preprint arXiv:1906.00910*, 2019. 3, 5

[5] Mohamed Ishmael Belghazi, Aristide Baratin, Sai Rajeswar, Sherjil Ozair, Yoshua Bengio, Aaron Courville, and R Devon Hjelm. Mine: mutual information neural estimation. *arXiv preprint arXiv:1801.04062*, 2018. 8

[6] Aurélien Bellet, Amaury Habrard, and Marc Sebban. Similarity learning for provably accurate sparse linear classification. *arXiv preprint arXiv:1206.6476*, 2012. 2

[7] Yoshua Bengio, Aaron Courville, and Pascal Vincent. Representation learning: A review and new perspectives. *TPAMI*, 2013. 2

[8] Avrim Blum and Tom Mitchell. Combining labeled and unlabeled data with co-training. In *COLT*. ACM, 1998. 2

[9] Piotr Bojanowski and Armand Joulin. Unsupervised learning by predicting noise. In *ICML*, 2017. 14

[10] Uta Buchler, Biagio Brattoli, and Bjorn Ommer. Improving spatiotemporal self-supervision by deep reinforcement learning. In *ECCV*, 2018. 6, 16

[11] Mathilde Caron, Piotr Bojanowski, Armand Joulin, and Matthijs Douze. Deep clustering for unsupervised learning of visual features. In *ECCV*, 2018. 5, 14

[12] Adam Coates, Andrew Ng, and Honglak Lee. An analysis of single-layer networks in unsupervised feature learning. In *AISTATS*, 2011. 5, 8, 13

[13] Corinna Cortes, Mehryar Mohri, and Afshin Rostamizadeh. Learning non-linear combinations of kernels. In *NIPS*, 2009. 2

[14] Ekin D Cubuk, Barret Zoph, Jonathon Shlens, and Quoc V Le. Randaugment: Practical data augmentation with no separate search. *arXiv preprint arXiv:1909.13719*, 2019. 5

[15] Hanneke EM Den Ouden, Peter Kok, and Floris P De Lange. How prediction errors shape perception, attention, and motivation. *Frontiers in psychology*, 2012. 1

[16] Jia Deng, Wei Dong, Richard Socher, Li-Jia Li, Kai Li, and Li Fei-Fei. Imagenet: A large-scale hierarchical image database. In *CVPR*, 2009. 5, 12, 14

[17] Carl Doersch, Abhinav Gupta, and Alexei A Efros. Unsupervised visual representation learning by context prediction. In *CVPR*, 2015. 5, 14

[18] Jeff Donahue, Philipp Krähenbühl, and Trevor Darrell. Adversarial feature learning. In *ICLR*, 2017. 5, 14

[19] Jeff Donahue and Karen Simonyan. Large scale adversarial representation learning. In *NIPS*, 2019. 5

[20] David Eigen and Rob Fergus. Predicting depth, surface normals and semantic labels with a common multi-scale convolutional architecture. In *ICCV*, 2015. 6

[21] Chuang Gan, Boqing Gong, Kun Liu, Hao Su, and Leonidas J Guibas. Geometry guided convolutional neural networks for self-supervised video representation learning. In *CVPR*, 2018. 6

[22] Spyros Gidaris, Praveer Singh, and Nikos Komodakis. Unsupervised representation learning by predicting image rotations. In *ICLR*, 2018. 5, 14

[23] Melvyn A Goodale and A David Milner. Separate visual pathways for perception and action. *Trends in neurosciences*, 1992. 6

[24] Ian Goodfellow, Jean Pouget-Abadie, Mehdi Mirza, Bing Xu, David Warde-Farley, Sherjil Ozair, Aaron Courville, and Yoshua Bengio. Generative adversarial nets. In *NIPS*, 2014. 1, 2, 3

[25] Michael Gutmann and Aapo Hyvärinen. Noise-contrastive estimation: A new estimation principle for unnormalized statistical models. In *AISTATS*, 2010. 3, 5, 12

[26] Raia Hadsell, Sumit Chopra, and Yann LeCun. Dimensionality reduction by learning an invariant mapping. In *CVPR*, 2006. 3

[27] Kaiming He, Haoqi Fan, Yuxin Wu, Saining Xie, and Ross Girshick. Momentum contrast for unsupervised visual representation learning. *arXiv preprint arXiv:1911.05722*, 2019. 5, 15

[28] Kaiming He, Xiangyu Zhang, Shaoqing Ren, and Jian Sun. Deep residual learning for image recognition. In *CVPR*, 2016. 5

[29] Olivier J Hénaff, Ali Razavi, Carl Doersch, SM Eslami, and Aaron van den Oord. Data-efficient image recognition with contrastive predictive coding. *arXiv preprint arXiv:1905.09272*, 2019. 3, 5

[30] Geoffrey E Hinton and Ruslan R Salakhutdinov. Reducing the dimensionality of data with neural networks. *science*, 2006. 2

[31] R Devon Hjelm, Alex Fedorov, Samuel Lavoie-Marchildon, Karan Grewal, Adam Trischler, and Yoshua Bengio. Learning deep representations by mutual information estimation and maximization. In *ICLR*, 2019. 3, 5, 6, 12, 13, 14, 15

[32] Jakob Hohwy. *The predictive mind*. Oxford University Press, 2013. 1

[33] Aapo Hyvärinen, Juha Karhunen, and Erkki Oja. *Independent component analysis*, volume 46. John Wiley & Sons, 2004. 2

[34] Phillip Isola, Jun-Yan Zhu, Tinghui Zhou, and Alexei A Efros. Image-to-image translation with conditional adversarial networks. In *CVPR*, 2017. 3

[35] Phillip Isola, Daniel Zoran, Dilip Krishnan, and Edward H Adelson. Learning visual groups from co-occurrences in space and time. *arXiv preprint arXiv:1511.06811*, 2015. 2

[36] Xu Ji, João F Henriques, and Andrea Vedaldi. Invariant information clustering for unsupervised image classification and segmentation. In *ICCV*, 2019. 3

[37] Ian Jolliffe. *Principal component analysis*. Springer, 2011. 2

[38] Kazuya Kawakami, Luyu Wang, Chris Dyer, Phil Blunsom, and Aaron van den Oord. Learning robust and multilingual speech representations. *arXiv preprint arXiv:2001.11128*, 2020. 3

[39] Celeste Kidd, Steven T Piantadosi, and Richard N Aslin. The goldilocks effect: Human infants allocate attention to visual sequences that are neither too simple nor too complex. *PloS one*, 2012. 8

[40] Diederik P Kingma and Max Welling. Auto-encoding variational bayes. *arXiv preprint arXiv:1312.6114*, 2013. 1, 2

[41] Alexander Kolesnikov, Xiaohua Zhai, and Lucas Beyer. Revisiting self-supervised visual representation learning. In *CVPR*, 2019. 5

[42] Philipp Krähenbühl, Carl Doersch, Jeff Donahue, and Trevor Darrell. Data-dependent initializations of convolutional neural networks. *arXiv preprint arXiv:1511.06856*, 2015. 5, 14

[43] Alex Krizhevsky, Ilya Sutskever, and Geoffrey E Hinton. Imagenet classification with deep convolutional neural networks. In *NIPS*, 2012. 5, 6, 15, 16

[44] Hsin-Ying Lee, Jia-Bin Huang, Maneesh Singh, and Ming-Hsuan Yang. Unsupervised representation learning by sorting sequences. In *ICCV*, 2017. 6, 16

[45] Yingming Li, Ming Yang, and Zhongfei Mark Zhang. A survey of multi-view representation learning. *TKDE*, 2018. 2

[46] Zelun Luo, Boya Peng, De-An Huang, Alexandre Alahi, and Li Fei-Fei. Unsupervised learning of long-term motion dynamics for videos. In *CVPR*, 2017. 6

[47] David McAllester and Karl Statos. Formal limitations on the measurement of mutual information. *arXiv preprint arXiv:1811.04251*, 2018. 4

[48] Antoine Miech, Jean-Baptiste Alayrac, Lucas Smaira, Ivan Laptev, Josef Sivic, and Andrew Zisserman. End-to-end learning of visual representations from uncurated instructional videos. In *CVPR*, 2020. 3

[49] Ishan Misra and Laurens van der Maaten. Self-supervised learning of pretext-invariant representations. *arXiv preprint arXiv:1912.01991*, 2019. 5, 15

[50] Ishan Misra, C Lawrence Zitnick, and Martial Hebert. Shuffle and learn: unsupervised learning using temporal order verification. In *ECCV*, 2016. 6, 16

[51] Andriy Mnih and Koray Kavukcuoglu. Learning word embeddings efficiently with noise-contrastive estimation. In *NIPS*, 2013. 3, 12

[52] Hossein Mobahi, Ronan Collobert, and Jason Weston. Deep learning from temporal coherence in video. In *ICML*, 2009. 6

[53] Pushmeet Kohli Nathan Silberman, Derek Hoiem and Rob Fergus. Indoor segmentation and support inference from rgbd images. In *ECCV*, 2012. 1, 6

[54] Mehdi Noroozi and Paolo Favaro. Unsupervised learning of visual representations by solving jigsaw puzzles. In *ECCV*. Springer, 2016. 5, 14

[55] Mehdi Noroozi, Hamed Pirsiavash, and Paolo Favaro. Representation learning by learning to count. In *ICCV*, 2017. 5, 14

[56] Aaron van den Oord, Nal Kalchbrenner, and Koray Kavukcuoglu. Pixel recurrent neural networks. *arXiv preprint arXiv:1601.06759*, 2016. 2

[57] Aaron van den Oord, Yazhe Li, and Oriol Vinyals. Representation learning with contrastive predictive coding. *arXiv preprint arXiv:1807.03748*, 2018. 2, 3, 4, 5, 12, 13, 14, 15

[58] Andrew Owens, Phillip Isola, Josh McDermott, Antonio Torralba, Edward H Adelson, and William T Freeman. Visually indicated sounds. In *CVPR*, 2016. 2, 3

[59] Adam Paszke, Sam Gross, Francisco Massa, Adam Lerer, James Bradbury, Gregory Chanan, Trevor Killeen, Zeming Lin, Natalia Gimelshein, Luca Antiga, et al. Pytorch: An imperative style, high-performance deep learning library. In *NIPS*, 2019. 5

[60] Deepak Pathak, Philipp Krahenbuhl, Jeff Donahue, Trevor Darrell, and Alexei A Efros. Context encoders: Feature learning by inpainting. In *CVPR*, 2016. 2

[61] AJ Piergiovanni, Anelia Angelova, and Michael S Ryoo. Evolving losses for unlabeled video representation learning. In *CVPR*, 2020. 3

[62] Ben Poole, Sherjil Ozair, Aaron van den Oord, Alexander A Alemi, and George Tucker. On variational bounds of mutual information. In *ICML*, 2019. 4

[63] Olaf Ronneberger, Philipp Fischer, and Thomas Brox. U-net: Convolutional networks for biomedical image segmentation. In *International Conference on Medical image computing and computer-assisted intervention*, 2015. 6

[64] Virginia Sa. Sensory modality segregation. In *NIPS*, 2004. 2

[65] Ruslan Salakhutdinov and Geoffrey Hinton. Deep boltzmann machines. In *AISTATS*, 2009. 1, 2

[66] Nawid Sayed, Biagio Brattoli, and Björn Ommer. Cross and learn: Cross-modal self-supervision. *arXiv preprint arXiv:1811.03879*, 2018. 6, 16

[67] Gerald E Schneider. Two visual systems. *Science*, 1969. 6

[68] Pierre Sermanet, Corey Lynch, Yevgen Chebotar, Jasmine Hsu, Eric Jang, Stefan Schaal, Sergey Levine, and Google Brain. Time-contrastive networks: Self-supervised learning from video. In *ICRA*, 2018. 2, 16

[69] Karen Simonyan and Andrew Zisserman. Two-stream convolutional networks for action recognition in videos. In *NIPS*, 2014. 6

[70] Linda Smith and Michael Gasser. The development of embodied cognition: Six lessons from babies. *Artificial life*, 2005. 1

[71] Paul Smolensky. Information processing in dynamical systems: Foundations of harmony theory. Technical report, Colorado Univ at Boulder Dept of Computer Science, 1986. 2

[72] Kihyuk Sohn. Improved deep metric learning with multi-class n-pair loss objective. In *NIPS*, 2016. 3, 5, 16

[73] Khurram Soomro, Amir Roshan Zamir, and Mubarak Shah. Ucf101: A dataset of 101 human actions classes from videos in the wild. *arXiv preprint arXiv:1212.0402*, 2012. 6

[74] Chen Sun, Fabien Baradel, Kevin Murphy, and Cordelia Schmid. Contrastive bidirectional transformer for temporal representation learning. *arXiv preprint arXiv:1906.05743*, 2019. 3

[75] Yonglong Tian, Dilip Krishnan, and Phillip Isola. Contrastive representation distillation. In *ICLR*, 2020. 3

[76] Michael Tschannen, Josip Djolonga, Marvin Ritter, Aravindh Mahendran, Neil Houlsby, Sylvain Gelly, and Mario Lucic. Self-supervised learning of video-induced visual invariances. *arXiv preprint arXiv:1912.02783*, 2019. 3

[77] Carl Vondrick, Hamed Pirsiavash, and Antonio Torralba. Generating videos with scene dynamics. In *NIPS*, 2016. 6

[78] Xiaolong Wang and Abhinav Gupta. Unsupervised learning of visual representations using videos. In *ICCV*, 2015. 2

[79] Zhirong Wu, Yuanjun Xiong, Stella X Yu, and Dahua Lin. Unsupervised feature learning via non-parametric instance discrimination. In *CVPR*, 2018. 2, 3, 5, 12, 14, 15, 16

[80] Chang Xu, Dacheng Tao, and Chao Xu. A survey on multi-view learning. *arXiv preprint arXiv:1304.5634*, 2013. 2

[81] Mang Ye, Xu Zhang, Pong C Yuen, and Shih-Fu Chang. Unsupervised embedding learning via invariant and spreading instance feature. In *CVPR*, 2019. 3

[82] Christopher Zach, Thomas Pock, and Horst Bischof. A duality based approach for realtime tv-l 1 optical flow. In *Joint pattern recognition symposium*, 2007. 6

[83] Liheng Zhang, Guo-Jun Qi, Liqiang Wang, and Jiebo Luo. Aet vs. aed: Unsupervised representation learning by auto-encoding transformations rather than data. In *CVPR*, 2019. 2, 5, 14

[84] Richard Zhang, Phillip Isola, and Alexei A Efros. Colorful image colorization. In *ECCV*. Springer, 2016. 2, 3, 5, 14

[85] Richard Zhang, Phillip Isola, and Alexei A Efros. Split-brain autoencoders: Unsupervised learning by cross-channel prediction. In *CVPR*, 2017. 2, 3, 5, 7, 14

[86] Chengxu Zhuang, Alex Andonian, and Daniel Yamins. Unsupervised learning from video with deep neural embeddings. *arXiv preprint arXiv:1905.11954*, 2019. 3

[87] Chengxu Zhuang, Alex Lin Zhai, and Daniel Yamins. Local aggregation for unsupervised learning of visual embeddings. *arXiv preprint arXiv:1903.12355*, 2019. 2, 5, 16

Table 6: The list of classes from ImageNet-100, which are randomly sampled from the original ImageNet-1k dataset [16]. This list can also be downloaded at: http://github.com/HobbitLong/CMC/blob/master/imagenet100.txt

List of ImageNet-100 classes				
n02869837	n01749939	n02488291	n02107142	n13037406
n02091831	n04517823	n04589890	n03062245	n01773797
n01735189	n07831146	n07753275	n03085013	n04485082
n02105505	n01983481	n02788148	n03530642	n04435653
n02086910	n02859443	n13040303	n03594734	n02085620
n02099849	n01558993	n04493381	n02109047	n04111531
n02877765	n04429376	n02009229	n01978455	n02106550
n01820546	n01692333	n07714571	n02974003	n02114855
n03785016	n03764736	n03775546	n02087046	n07836838
n04099969	n04592741	n03891251	n02701002	n03379051
n02259212	n07715103	n03947888	n04026417	n02326432
n03637318	n01980166	n02113799	n02086240	n03903868
n02483362	n04127249	n02089973	n03017168	n02093428
n02804414	n02396427	n04418357	n02172182	n01729322
n02113978	n03787032	n02089867	n02119022	n03777754
n04238763	n02231487	n03032252	n02138441	n02104029
n03837869	n03494278	n04136333	n03794056	n03492542
n02018207	n04067472	n03930630	n03584829	n02123045
n04229816	n02100583	n03642806	n04336792	n03259280
n02116738	n02108089	n03424325	n01855672	n02090622

A. ImageNet-100 Proposed in this Paper

In this paper, we proposed a subset of ImageNet that contains randomly selected 100 classes for ablation study as well as hyper-parameter tuning. To ease a relevant study in the future, we release the list of these categories that we consistently used throughout all our experiments, as summarized in Table 6.

B. Contrastive Loss

B.1. NCE approximation for high-dimensional softmax corss-entropy

In addition to the subsampled (m+1)-way softmax cross-entropy, Noise-Contrastive Estimation (NCE [25]) is another way to approximate the N-way (N is the dataset size) softmax cross entropy full softmax in Eqn 2. Compared with the (m+1)-way softmax cross-entropy, NCE is computationally faster and may result in slightly worse performance in standard linear evaluation. It has been used in [51, 79][1]. We depict its general idea as below.

Given an anchor v_1^i from V_1, the probablity that an atom $v_2 \in \{v_2^j | j = 1, 2, ..., N\}$ from V_2 is the best match of v_1^i, using the score h_θ is given by:

$$p(v_2|v_1^i) = \frac{h_\theta(\{v_1^i, v_2\})}{\sum_{j=1}^{N} h_\theta(\{v_1^i, v_2^j\})} \tag{9}$$

where the normalization factor $Z = \sum_{j=1}^{N} h_\theta(\{v_1^i, v_2^j\})$ is expensive to compute for large N.

NCE [25] is an effective way to estimate *unnormalized* statistical models. NCE fits a density model p to data distributed as (unknown) distribution p_d, by using a binary classifier to distinguish it from noise samples distributed as p_n. To learn $p(v_2|v_1^i)$, we use a binary classifier, which treats v_2^i as the data (or positive) sample when given v_1^i. The noise distribution $p_n(\cdot|v_1^i)$ we choose here is a uniform distribution over all atoms from V_2, i.e., $p_n(\cdot|v_1^i) = p_n(\cdot) = 1/N$. If we sample m noise samples to pair with each data sample, the posterior probability that a given atom v_2 comes from the data distribution is:

$$P(D = 1|v_2; v_1^i) = \frac{p_d(v_2|v_1^i)}{p_d(v_2|v_1^i) + m p_n(v_2|v_1^i)} \tag{10}$$

and we estimate this probability by replacing $p_d(v_2|v_1^i)$ with our *unnormalized* model distribution $h_\theta(v_1^i, v_2)/Z_0$, where Z_0 is a constant estimated from the first batch. Minimizing the negative log-posterior probability of correct labels D over data and noise samples yields our final objective, which is the NCE-based approximation of Eq. 2 ($\hat{p}$ is the empirical data distribution):

$$\begin{aligned} L_{NCE} = \; & - \mathop{\mathbb{E}}_{v_1^i \sim \hat{p}(v_1)} \Big\{ \mathop{\mathbb{E}}_{v_2 \sim \hat{p}(\cdot|v_1^i)} \big[\log(P(D = 1|v_2; v_1^i))\big] \\ & + \; m \mathop{\mathbb{E}}_{v_2 \sim p_n(\cdot|v_1^i)} \big[\log(P(D = 0|v_2; v_1^i))\big] \Big\} \end{aligned} \tag{11}$$

B.2. Contrasting Sub-patches

Instead of contrasting features from the last layer, patch-based method [31] contrasts feature from the last layer with features from previous layers, hence increasing the number of negative pairs. For instance, we use features from the last layer of f_{θ_1} to contrast with feature points from feature maps produced by the first several conv layers of f_{θ_2}. This is equivalent to contrast between global patch from one view with local patches from the other view. In this fashion, we directly perform $m + 1$ way softmax classification, the same as [57, 31] for a fair comparison in Sec. D.1.

Such patch-based contrastive loss is computed within each mini-batch and does not require a memory bank. Therefore, deploying it in parallel training schemes is easy and flexible. However, patch-based contrastive loss usually yields suboptimal results compared to NCE-based contrastive loss, according to our experiments.

C. Proofs

We prove that: (a) the optimal score function $h_\theta^*(\{v_1, v_2\})$ is proportional to density ratio between the joint distribution

[1] Confusingly, the literature has previously referred to Eqn.2 as "InfoNCE" [57]. Our NCE approximation *does not* refer to the allusion to NCE in the name "InfoNCE". Rather we are here describing an NCE approximation to the "InfoNCE" softmax objective.

$p(v_1, v_2)$ and product of marginals $p(v_1)p(v_2)$, as shown in Eq. 5; (b) Minimizing the contrastive loss $\mathcal{L}_{contrast}$ maxmizes a lower bound on the mutual information between two views, as shown in Eq. 6.

We will use the most general formula of contrastive loss $\mathcal{L}_{contrast}$ shown in Eq. 1 for our derivation. But we note that replacing $\mathcal{L}_{contrast}$ with $\mathcal{L}_{contrast}^{V_1,V_2}$ is straightforward. The overall proof follows a similar derivation introduced in [57].

C.1. Score function as density ratio estimator

We first show that the optimal score function $h_\theta^*(\{v_1, v_2\})$ that minimizes Eq. 1 is proportional to the density ratio between joint distribution and product of marginals, shown as Eq. 5. For notation convenience, we denote $p(v_1, v_2)$ as data distribution $p_d(\cdot)$ and $p(v_1)p(v_2)$ as noise distribution $p_n(\cdot)$. The loss in Eq. 1 is indeed a cross-entropy loss of classifying the correct positive pair out from the given set S. Without loss of generality, we assume the first pair (v_1^0, v_2^0) in S is positive or congruent and all others $(v_1^i, v_2^i), i = 1, 2, ..., k$ are negative or incongruent. The optimal probability for the loss, $p(pos = 0|S)$, should depict the fact that (v_1^0, v_2^0) comes from the data distribution $p_d(\cdot)$ while all other pairs come from the noise distribution $p_n(\cdot)$. Therefore,

$$\begin{aligned} p(pos = 0|S) &= \frac{p_d(v_1^0, v_2^0) \prod_{i=1}^k p_n(v_1^i, v_2^i)}{\sum_{j=0}^k p_d(v_1^j, v_2^j) \prod_{i\neq j} p_n(v_1^i, v_2^i)} \\ &= \frac{p(v_1^0, v_2^0) \prod_{i=1}^k p(v_1^i)p(v_2^i)}{\sum_{j=0}^k p(v_1^j, v_2^j) \prod_{i\neq j} p(v_1^i)p(v_2^i)} \\ &= \frac{\frac{p(v_1^0, v_2^0)}{p(v_1^0)p(v_2^0)}}{\sum_{j=0}^k \frac{p(v_1^k, v_2^k)}{p(v_1^k)p(v_2^k)}} \end{aligned}$$

where we plug in the definition of $p_d(\cdot)$ and $p_n(\cdot)$, and divide $\prod_{i=0}^k p(v_1^i)p(v_2^2)$ for both the numerator and denominator. By comparing above equation with the loss function in Eq. 1, we can see that the optimal score function $h_\theta^*(\{v_1, v_2\})$ is proportional to the density ratio $\frac{p(v_1,v_2)}{p(v_1)p(v_2)}$. The above derivation is agnostic to which layer the score function starts from, e.g., h can be defined on either the raw input (v_1, v_2) or the latent representation (z_1, z_2). As we care more about the property of the latent representation, for the following derivation we will use $h^*(\{z_1, z_2\})$, which is proportional to $\frac{p(z_1,z_2)}{p(z_1)p(z_2)}$.

C.2. Maximizing lower bound on MI

Now we substitute the score function in Eq. 1 with the above density ratio, and the optimal loss objective $\mathcal{L}_{contrast}^{opt}$ becomes:

$$\begin{aligned} \mathcal{L}_{contrast}^{opt} &= -\mathop{\mathbb{E}}_S \log \left[\frac{h^*(\{z_1^0, z_2^0\})}{\sum_{i=0}^k h^*(\{z_1^i, z_2^i\})} \right] \\ &= -\mathop{\mathbb{E}}_S \log \left[\frac{\frac{p(z_1^0, z_2^0)}{p(z_1^0)p(z_2^0)}}{\sum_{i=0}^k \frac{p(z_1^i, z_2^i)}{p(z_1^i)p(z_2^i)}} \right] \\ &= \mathop{\mathbb{E}}_S \log \left[1 + \frac{p(z_1^0)p(z_2^0)}{p(z_1^0, z_2^0)} \sum_{i=1}^k \frac{p(z_1^i, z_2^i)}{p(z_1^i)p(z_2^i)} \right] \\ &\approx \mathop{\mathbb{E}}_S \log \left[1 + \frac{p(z_1^0)p(z_2^0)}{p(z_1^0, z_2^0)} k \mathop{\mathbb{E}}_{z_1} \left[\frac{p(z_1|z_2)}{p(z_1)} \right] \right] \\ &= \mathop{\mathbb{E}}_S \log \left[1 + \frac{p(z_1^0)p(z_2^0)}{p(z_1^0, z_2^0)} k \right] \\ &\geq \log(k) - \mathop{\mathbb{E}}_S \log \left[\frac{p(z_1^0, z_2^0)}{p(z_1^0)p(z_2^0)} \right] \\ &= \log(k) - \mathop{\mathbb{E}}_{(z_1,z_2)\sim p_{z_1,z_2}(\cdot)} \log \left[\frac{p(z_1, z_2)}{p(z_1)p(z_2)} \right] \\ &= \log(k) - I(z_1; z_2) \end{aligned}$$

Therefore, for any two views V_i and V_j, we have $I(z_i; z_j) \geq \log(k) - \mathcal{L}_{contrast}^{opt}(V_i, V_j)$. As the k increases, the approximation step becomes more accurate. Given any k, minimizing $\mathcal{L}_k(V_i, V_j)$ maximizes the lower bound on the mutual information $I(z_i; z_j)$. We should note that increasing k to infinity does not always lead to a higher lower bound. While $\log(k)$ increases with a larger k, the optimization problem becomes harder and $\mathcal{L}_k(V_i, V_j)$ also increases.

D. Additional Experiments

D.1. CMC on STL-10

STL-10 [12] is an image recognition dataset designed for developing unsupervised or self-supervised learning algorithms. It consists of 100000 unlabeled training 96×96 RGB image samples and 500 labeled samples for each of the 10 classes.

Setup. We adopt the same data augmentation strategy and network architecture as those in DIM [31]. A variant of AlexNet takes as input 64×64 images, which are randomly cropped and horizontally flipped from the original 96×96 size images. For a fair comparison with DIM, we also train our model in a patch-based contrastive fashion during unsupervised pre-training. With the weights of the pre-trained encoder frozen, a two-layer fully connected network with 200 hidden units is trained on top of different layers for 100 epochs to perform 10-way classification. We also investigated the strided crop strategy of CPC [57]. Fixed sized overlapping patches of size 16×16 with an overlap of 8 pixels are cropped and fed into the network separately. This ensures that features of one patch contain minimal information from neighbouring patches; and increases the available

number of negative pairs for the contrastive loss. Additionally, we include NCE-based contrastive training and linear classifier evaluation.

Comparison. We compare CMC with the state of the art unsupervised methods in Table 7. Three columns are shown: the conv5 and fc7 columns use respectively these layers of AlexNet as the encoder (again remembering that we split across channels for L and ab views). For these two columns we can compare against the all methods except CPC, since CPC does not report these numbers in their paper [31]. In the Strided Crop setup, we only compare against the approaches that use contrastive learning, DIM and CPC, since this method was only used by those works. We note that in Table 7 for all the methods except SplitBrain, we report numbers are shown in the original paper. For SplitBrain, we reimplemented their model faithfully and report numbers based on our reimplementation (we verified the accuracy of our SplitBrain code by the fact that we get very similar results with our reimpementation as in the original paper [85] for ImageNet experiments, see below).

The family of contrastive learning methods, such as DIM, CPC, and CMC, achieve higher classification accuracy than other methods such as SplitBrain that use predictive learning; or BiGAN that use adversarial learning. CMC significantly outperforms DIM and CPC in all cases. We hypothesize that this outperformance results from the modeling of cross-view mutual information, where view-specific noisy details are discarded. Another head-to-head comparison happens between CMC and SplitBrain, both of which modeling images as seprated L and ab streams; we achieve a nearly 8% absolute improvement for conv5 and 17% improvement for fc5. Finally, we notice that the predictive learning methods suffer from a big drop in performance when the encoding layer is switched from conv5 to fc7. On the other hand, the contrastive learning approaches are much more stable across layers, suggesting that the mutual information maximization paradigm learns more semantically meaningful representations shared by the different views. From a practical perspective, this is a significant advantage as the selection of specific layers should ideally not change downstream performance by too much.

In this experiments we used AlexNet as backbone. Switching to more powerful networks such as ResNets is likely to further improve the representation quality.

D.2. CMC on ImageNet with AlexNet

ImageNet [16] consists of 1000 image classes and is frequently considered as a testbed for unsupervised representation learning algorithms.

To compare with other methods, we adopt standard AlexNet and split it into two encoders. Because of splitting, each layer only connects to half of the neurons in the previous layer, and therefore the number of parameters in our model halves. We remove local response layer and add batch normalization to each layer. For the memory-based CMC model, we adopt ideas from [79] for computing and storing a memory. We retrieve 4096 negative pairs from the memory bank to contrast each positive pair (the effect of the number of negatives is shown in Sec. D.3). The training details are present in Sec. E.2.

Method	classifier	conv5	fc7	Strided Crop
AE	MLP	62.19	55.78	-
NAT [9]		64.32	61.43	-
BiGAN [18]		71.53	67.18	-
SplitBrain† [85]		72.35	63.15	-
DIM [31]	MLP	72.57	70.00	78.21
CPC [57]		-	-	77.81
CMC†(Patch)	Linear	76.65	79.25	82.58
CMC†(Patch)	MLP	80.14	80.11	**83.43**
CMC†(NCE)	Linear	83.28	86.66	-
CMC†(NCE)	MLP	**84.64**	**86.88**	-
Supervised		68.70		

Table 7: Classification accuracies on STL-10 by using a two layer MLP as classifier for evaluating the representations learned by a small **AlexNet**. For all methods we compare against, we include the numbers that are reported in the DIM [31] paper, except for SplitBrain, which is our reimplementation. Methods marked with † have half the number of parameters because of splitting.

Method	ImageNet Classification Accuracy				
	conv1	conv2	conv3	conv4	conv5
ImageNet-Labels	19.3	36.3	44.2	48.3	50.5
Random	11.6	17.1	16.9	16.3	14.1
Data-Init [42]	17.5	23.0	24.5	23.2	20.6
Context [17]	16.2	23.3	30.2	31.7	29.6
Colorization [84]	13.1	24.8	31.0	32.6	31.8
Jigsaw [54]	19.2	30.1	34.7	33.9	28.3
BiGAN [18]	17.7	24.5	31.0	29.9	28.0
SplitBrain† [85]	17.7	29.3	35.4	35.2	32.8
Counting [55]	18.0	30.6	34.3	32.5	25.7
Inst-Dis [79]	16.8	26.5	31.8	34.1	35.6
RotNet [22]	18.8	31.7	38.7	38.2	36.5
DeepCluster [11]	12.9	29.2	38.2	39.8	36.1
AET [83]	**19.3**	32.8	**40.6**	39.7	37.7
CMC†($\{Y, DbDr\}$)	18.3	**33.7**	38.3	**40.5**	**42.8**

Table 8: Top-1 classification accuracy on 1000 classes of ImageNet [16] with *single* crop. We compare our CMC method with other unsupervised representation learning approaches by training 1000-way logistic regression classifiers on top of the feature maps of each layer, as proposed by [84]. Methods marked with † only have half the number of parameters compared to others, because of splitting.

Table 8 shows the results of comparing the CMC against other models, both predictive and contrastive. Our CMC is

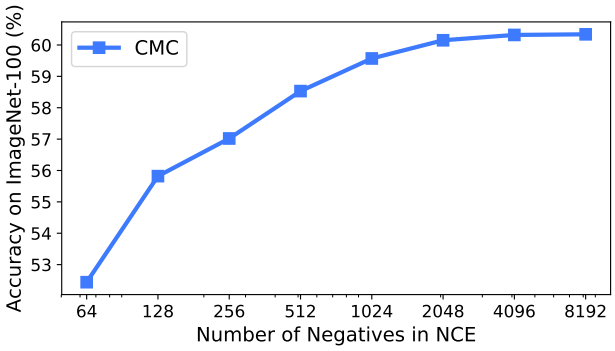

Figure 6: We plot the number of negative examples m in NCE-based contrastive loss against the accuracy for 100 randomly chosen classes of Imagenet 100. It is seen that the accuracy steadily increases with m.

the best among all these methods; futhermore CMC tends to perform better at higher convolutional layers, similar to another contrasting-based model Inst-Dis [79].

D.3. Number of negatives

Effect of the number of negative samples. We investigate the relationship between the number of negative pairs m in NCE-based loss and the downstream classification accuracy on a randomly chosen subset of 100 classes of Imagenet (the same set of classes is used for any number of negative pairs). We train a 100-way linear classifier using CMC pre-trained features with varying number of negative pairs, starting from 64 pairs upto 8192 (in multiples of 2). Fig. 6 shows that the accuracy of the resulting classifier steadily increases but saturates at around 60.3% with $m = 4096$ samples. We used AlexNet and the NCE approximation in this study ($(m+1)$-way softmax cross entropy, a.k.a. InfoNCE, also follow a similar trend).

D.4. Compatibility with other methods

To test the compatibility of CMC with mechanisms proposed in other self-supervised learning methods, we consider combining CMC with MoCo [27] (*i.e.*, switching from memory bank [79] to momentum encoder) and PIRL [49] (*i.e.*, applying a second JigSaw branch). In this setup, we perform both unsupervised pre-training and linear evaluation on the same ImageNet-100 subset as above. We use the same contrastive loss objective function and training recipe for all methods, to ensure a head-to-head comparison. Specifically, we pre-train for 240 epochs with learning rate initialized as 0.03 and decayed with cosine annealing schedule.

Table 9 summarizes the results. We observe that combining CMC with the MoCo mechanism or JigSaw branch in PIRL can consistently improve the performance, verifying that they are compatible.

Method	# of Params	Top-1 Acc
MoCo	24M	73.5
PIRL	24M	75.1
CMC	12M	75.6
CMC + MoCo	12M	77.2 **(+1.6)**
CMC + PIRL	12M	78.0 **(+2.4)**
CMC + MoCo + PIRL	12M	79.3 **(+3.7)**
CMC + MoCo + PIRL + RA	12M	81.5 **(+5.9)**

Table 9: Compatibility of CMC with other mthods. We pre-train and evaluate on ImageNet-100 subset with top-1 accuracy reported. Specifically, we combine CMC with MoCo (*i.e.*, switching from memory bank to momentum encoder), PIRL (*i.e.*, applying a second JigSaw branch), or both. Consistent improvement is observed with a ResNet-50. RA stands for RandAugment.

Half of AlexNet[43] for STL-10					
Layer	**X**	**C**	**K**	**S**	**P**
data	64	*	–	–	–
conv1	64	48	3	1	1
pool1	31	48	3	2	0
conv2	31	96	3	1	1
pool2	15	96	3	2	0
conv3	15	192	3	1	1
conv4	15	192	3	1	1
conv5	15	96	3	1	1
pool5	7	96	3	2	0
fc6	1	2048	7	1	0
fc7	1	2048	1	1	0
fc8	1	64	1	1	0

Table 10: **The variant of AlexNet architecture used in our CMC for STL-10 (only half is present here due to splitting).** **X** spatial resolution of layer, **C** number of channels in layer; **K** `conv` or `pool` kernel size; **S** computation stride; **P** padding; * channel size is dependent on the input source, e.g. 1 for L channel and 2 for ab channel.

E. Implementation Details

E.1. STL-10

For a fair comparison with DIM [31] and CPC [57], we adopt the same architecture as that used in DIM and split it into two encoders, each shown as in Table 10. For the implementation of the score function, we adopt similar "encoder-and-dot-product" strategy, which is tantamount to a bilinear model.

In the patch-based contrastive learning stage, we use Adam optimizer with an initial learning rate of 0.001, $\beta_1 = 0.5$, $\beta_2 = 0.999$. We train for a total of 200 epochs with learning rate decayed by 0.2 after 120 and 160 epochs. In the non-linear classifier evaluation stage, we use the same

optimizer setting. For the NCE-based contrastive learning stage, we train for 320 epochs with the learning rate initialized as 0.03 and further decayed by 10 for every 40 epochs after the first 200 epochs. The temperature τ is set as 0.1. In general, $\tau \in [0.05, 0.2]$ works reasonably well.

E.2. ImageNet

For patch-based contrastive loss, we use the same optimizer setting as in Sec. E.1 except that the learning rate is initialized as 0.01.

For NCE-basd contrastive loss in both full ImageNet and ImageNet100 experiments present in Sec. D.3, the encoder architecture used for either L or ab channels is shown in Table 11. In the unsupervised learning stage of AlexNet, we use SGD to train the network for a total of 200 epochs. The temperature τ is set as 0.07 by following previous work [79]. The learning rate is initialized as 0.03 with a decay of 10 for every 40 epochs after the first 120 epochs. Weight decay is set as 10^{-4} and momentum is kept as 0.9. For the linear classification stage, we train for 100 epochs. The learning rate is initialized as 0.1 and decayed by 0.2 every 15 epochs after the first 60 epochs. We set weight decay as 0 and momentum as 0.9.

For ResNets in CMC stage, instead of using step decay, we choose cosine annealing to gradually decrease the learning rate. In the linear evaluation stage, we train for 100 epochs. The learning rate is initialized as 30 for ResNet-50 and ResNet-101, and 50 for ResNet-50 x2. It is decayed by 0.2 every 15 epochs after the first 60 epochs. We set weight decay as 0 and momentum as 0.9.

Half of AlexNet[43] for ImageNet					
Layer	**X**	**C**	**K**	**S**	**P**
data	224	*	–	–	–
conv1	55	48	11	4	2
pool1	27	48	3	2	0
conv2	27	128	5	1	2
pool2	13	128	3	2	0
conv3	13	192	3	1	1
conv4	13	192	3	1	1
conv5	13	128	3	1	1
pool5	6	128	3	2	0
fc6	1	2048	6	1	0
fc7	1	2048	1	1	0
fc8	1	128	1	1	0

Table 11: **AlexNet architecture used in CMC for ImageNet (only half is present here due to splitting)**. **X** spatial resolution of layer, **C** number of channels in layer; **K** `conv` or `pool` kernel size; **S** computation stride; **P** padding; * channel size is dependent on the input source, e.g. 1 for L channel and 2 for ab channel.

E.3. UCF101 and HMDB51

Following previous work [50, 44, 66, 10], we use CaffeNet for the video experiments. We tailor the network and use features from the fc6 layer for contrastive learning. Dropout of 0.5 is used to alleviate overfitting.

E.4. NYU Depth-V2

While experimenting with different views on NYU Depth-V2 dataset, we encode the features from patches with a size of 128×128. The detailed architecture is shown in Table 12. In the unsupervised training stage, we use Adam optimizer with an initial learning rate of 0.001, $\beta_1 = 0.5$, $\beta_2 = 0.999$. We train for a total of 3000 epochs with learning rate decayed by 0.2 after 2000, 2400, and 2800 epochs. For the downstream semantic segmentation task, we use the same optimizer setting but train for fewer epochs. We only train 200 epochs for CMC pre-trained models, and train 1000 epochs for the *Random* and *Supervised* baselines until convergence. For the classification task evaluated on STL-10, we use the same optimizer setting as in Sec. E.1 to report numbers.

Encoder Architecture on NYU					
Layer	**X**	**C**	**K**	**S**	**P**
data	128	*	–	–	–
conv1	64	64	8	2	3
pool1	32	64	2	2	0
conv2	16	128	4	2	1
conv3	8	256	4	2	1
conv4	8	256	3	1	1
conv5	4	512	4	2	1
fc6	1	512	4	1	0
fc7	1	256	1	1	0

Table 12: **Encoder architecture used in our CMC for playing with different views on NYU Depth-V2**. **X** spatial resolution of layer, **C** number of channels in layer; **K** `conv` or `pool` kernel size; **S** computation stride; **P** padding; * channel size is dependent on the input source, e.g. 1 for L, 2 for ab, 1 for depth, 3 for surface normal, and 1 for segmentation map.

F. Change Log

arXiv v2 Added references to Time Contrastive Networks [68] and Local Aggregation [87]. Fixed Typos.

arXiv v3 Added analysis of effect of mutual information, updated results, and rearranged the contents.

arXiv v4 Added reference to the original k-pair loss [72] and other related work. Cited some recent works to reflect progresses after our v1 version. We also removed Fast AutoAugment and rearranged the contents.

arXiv v5 Added the list of ImageNet-100 proposed in this paper, and the compatibility of CMC with other methods.